Lattice effects in cubic $La_2Mo_2O_9$: Effect of vacuum and correlation with transport properties

Cristina Tealdi[a,*], Lorenzo Malavasi[a], Clemens Ritter[b], Giorgio Flor[a], Giorgio Costa[c]

[a]*Dipartimento di Chimica Fisica "M.Rolla", Università di Pavia, Viale Taramelli 16, 27100 Pavia, Italy*
[b]*Institute Laue-Langevin, Boite Postale 156, F-38042 Grenoble, France*
[c]*Dipartimento di Chimica e Chimica Industriale, Università di Genova, Via Dodecaneso 31, 16146 Genova, Italy*

Abstract

This study aims to investigate correlations between lattice effects and transport properties in cubic $La_2Mo_2O_9$. High temperature neutron diffraction data, recorded in air and under vacuum, are used to follow the evolution with temperature of selected structural parameters, *i.e.* bond lengths and angles. Results suggest a possible correlation with the experimentally observed decrease of the activation energy for oxygen migration at high temperature. The effect on the structural properties of the low oxygen partial pressure used during the measurements in vacuum is negligible and this represents a valuable information in view of possible applications of the material in solid state devices.
© 2008 Elsevier Inc. All rights reserved.

Keywords: Neutron diffraction; Ionic conductivity

1. Introduction

The LAMOX family of fast ion conductors, based on the parent compound $La_2Mo_2O_9$, has been lately the subject of intense research. These materials are competitive with existing electrolytes (such as YSZ) at temperatures above $600\,°C$, where a transition from a monoclinic (α) to a cubic (β) phase occurs; connected with this phase transition there is a drastic improvement in the ionic conductivity by approximately two orders of magnitude, such that a value of $0.03\,S\,cm^{-1}$ can be achieved at $\sim720\,°C$. From the first claims of its performance as solid electrolyte [1,2], a considerable amount of work has been directed to the possibility to overcome both the phase transition and the reducibility of this material, with the perspective of technological applications at lower temperature [3–9].

From a basic point of view, one of the most interesting and debated point to consider is the mechanism of oxygen transport throughout the lattice and its relationship with the crystal structure of this material. The structural properties of $La_2Mo_2O_9$ at high temperature were first investigated by Goutenoire et al. by powder neutron diffraction [10,11]. The β-high conductive form of $La_2Mo_2O_9$ crystallizes in the cubic space group $P2_13$. Large anisotropic thermal parameters and partial site occupancies characterize two of the three crystallographic independent oxygen sites. Recently the structure of the monoclinic α form of $La_2Mo_2O_9$ has been determined [12]. The material, despite its simple chemical formula, has a remarkable 312 crystallographically unique atoms and is thus one of the most complex oxide structure reported to date. Our recent paper [13] based on a neutron PDF analysis of pure $La_2Mo_2O_9$ below and above the phase transition has highlighted the fact that the transition from the monoclinic to the cubic phase is a transition from a static to a dynamic distribution of the oxygen defects while preserving the monoclinic local structure. This agrees with the observation by Evans and co-authors that the β form of $La_2Mo_2O_9$ corresponds to a time-averaged version of the room-temperature structure, which has given an important input for the comprehension of the mechanism of oxygen diffusion in β-$La_2Mo_2O_9$.

---

*Corresponding author. Fax: +39 382 907575.

E-mail address: cristina.tealdi@unipv.it (C. Tealdi).

Earlier works, based on mechanical and dielectric relaxation studies, have suggested the possibility that the oxygen vacancies migration path involves all of the three oxygen sites, including the fully occupied O1 site [14–17]. However, the large anisotropic thermal parameters and partial site occupancies which characterize the O2 and O3 sites of this structure, associated with the short oxygen–oxygen distances between these two atoms, makes the conduction path between O2 and O3 more likely [11,12,18,19]. These results are also supported by oxygen diffusion measurements [19]. On the other hand, recent molecular dynamics studies [20] have resumed the idea that two diffusion channels are present in β-La$_2$Mo$_2$O$_9$: a first one characterized by low activation energy and short migration lengths which involves only O2 and O3 sites and a second one with larger activation energy and long migration lengths involving all the three crystallographic oxygen sites.

A deep structural analysis can suggest interesting points on the transport properties of this material and possibly discern some debating points. For this purpose a useful type of structural representation has been introduced [21], which differs from the conventional representation in terms of coordination polyhedra of cations. The new description of the β-La$_2$Mo$_2$O$_9$ structure follows the alternative approach of O'Keeffe and Hyde [22] and puts emphasis on the coordination sphere of anions. According to this approach, it is possible to construct a rigid structural framework built up from [O1LaMo] tetrahedral units surrounded by partly delocalized oxide ions on O2 and O3 sites. Fig. 1 shows a representation of the full structure
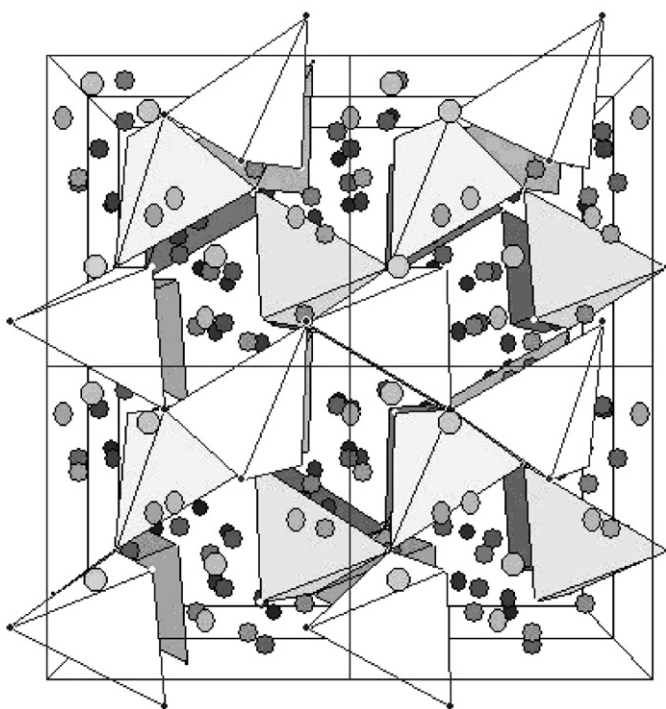

Fig. 1. Description of the β-La$_2$Mo$_2$O$_9$ as a rigid framework of [O1LaMo] with O2 and O3 oxide ions sites embedded in its tunnels.

according to this alternative description. The [O1LaMo] framework shapes tunnels along the cubic cell axes, in which oxide ions are located on O2 and O3 sites. This open structure is more likely to reflect the basic nature of the β-La$_2$Mo$_2$O$_9$ crystal structure and transport properties. The short O2–O3 and O3–O3 distances are believed to be at the basis of the easy oxygen migration throughout this structure. Earlier works [9,23] have underlined the presence, at high temperature, of a well-evident non-Arrhenius behaviour in the conductivity plots of pure and substituted La$_2$Mo$_2$O$_9$. A recent work [24] from Lacorre's group, based on molecular dynamic calculations, has suggested a possible correlation between the non-Arrenhius behaviour typical of these phases and a possible rotation and tilting of the anti-tetrahedral units with temperature. This hypothesis has been tested using molecular dynamic simulations and has not been compared, up to now, with experimental data acquired in a wide temperature range.

In an attempt to better understand the correlations between structural and transport properties of this fascinating oxide, we have undertaken a structural study based on neutron diffraction data. The thermal evolution of a sample of nominal composition (La$_{0.95}$K$_{0.05}$)$_2$Mo$_2$O$_{8.9}$ has been studied by means of neutron diffraction in the temperature range between room temperature and 700 °C; this kind of substitution on the La site ensures for this sample the stabilization of the cubic β-phase at room temperature. This sample has been the subject of a previous experimental work [9] which has highlighted the presence of a well evident non-Arrhenius behaviour for this sample at high temperature, in agreement with other reports in this field [23,25].

By following the evolution with temperature of some selected structural parameters, we expect to be able to give new information on structure/transport properties correlations for the LAMOX family of oxide ion conductors. The main idea beyond this study is, first of all, to compare our experimental results with the model proposed by Lacorre's group [24] which could partially explain important structural/transport relationships in these compounds. Moreover, this study focuses on the comparison between structural data acquired both in air and under vacuum. This is expected to represent a valuable information in view of possible application of the material in solid state devices since any relevant structural modification associated with the change in oxygen partial pressure may affect the mechanical stability of the system.

Although previous neutron or X-ray diffraction studies on selected La$_2$Mo$_2$O$_9$ samples have been carried out, these compared mainly structural results before and after the phase transition [10,18] or focused on the evolution with temperature of cell parameter [5,11]. To the best of our knowledge this is the first neutron diffraction study that presents a comparison between structural data obtained in air and in vacuum and that follows the evolution with temperature of cell parameters as well as bond lengths and relevant angles.

2. Experimental

2.1. Synthesis

A sample of nominal composition $(La_{0.95}K_{0.05})_2Mo_2O_{8.9}$ has been prepared by means of a slightly modified Pechini route. $La(NO_3)_3 \cdot 6H_2O$ (Aldrich, 99.99%), $(NH_4)_6Mo_7O_{24} \cdot 4H_2O$ (Aldrich, >99%) and KNO_3 (Aldrich, 99.99%) were used as starting materials, citric acid as the chelating agent and ethylene glycol to enhance the gelation process. The pH of the solution was adjusted to approximately 8 in order to promote the complexation of the metal ions. The solution was dried slowly at 70 °C, continuously subjected to vigorous stirring. After the complete evaporation of the water, the dried gel obtained was first heated at 500 °C to burn out the organic matter, then at 900 °C to improve the crystallization grade of the compound before finally being slowly cooled to room temperature. Room temperature X-ray powder diffraction (XRPD) patterns acquired with a Bruker D8 Advance diffractometer confirm the stabilization of the cubic β phase for this composition, in agreement with the available literature data [9,17].

2.2. Neutron data acquisition and structural refinement

Neutron powder patterns have been acquired with the D1A diffractometer at ILL (*Institute Laue-Langevin*, Grenoble, France) at $\lambda \sim 1.39$ Å in the 2θ range $-22 < 2\theta < 160$, with steps of 0.1°. A first set of measurements has been performed at variable temperatures (ranging from room temperature up to 700 °C), using a vanadium furnace under vacuum (oxygen partial pressure: 10^{-6} atm). A set of complementary data has been acquired in the temperature range between room temperature and 700 °C using a silica glass container under static air.

Thermogravimetric analysis (shown as Supplementary Information) performed on ~ 1 g of sample under vacuum (10^{-3} bar) in a metallic container from room temperature up to 1100 °C shows the stability of the sample in the measurements conditions. In particular, the sample underwent an isothermal step at 800 °C for 10 h. The measured oxygen loss corresponds at a $\delta = -0.005$ when reported to the 9 oxygen per formula, which is unlikely to have a relevant effect on the mean, long range characterization of the material.

All the neutron patterns have been analysed according to the Rietveld method [26,27], by means of the FULLPROF software package [30]. Cell parameters, atomic positions, anisotropic thermal factors, zero point error and profile parameters have been refined. The background was fitted with an interpolation between fixed points chosen outside Bragg peaks; the background due to the empty quartz tube (recorded at the same temperatures of the samples) was subtracted from the neutron patterns of the samples.

3. Results

All the neutron patterns have been indexed in the cubic space group $P2_13$. In Table 1 the refined lattice constants and atomic positions obtained from the data recorded under air are listed for the five temperatures considered, while Fig. 2 shows a representative example of a refined diffraction pattern recorded under vacuum.

The evolution of the unit cell volume for the cubic $(La_{0.95}K_{0.05})_2Mo_2O_{8.9}$ sample is presented in Fig. 3. As expected, the size of the unit cell increases as a function of temperature. A careful inspection of the data might reveal the presence of a small deviation from the linear trend for temperatures higher than approximately 400 °C. In the inset of Fig. 3 the relative extra volume expansion in excess to the regular thermal expansion, as calculated from the extrapolation at high temperature of the linear expansion below 400 °C, is presented for the data collected in air. Such a behaviour, already observed in several cubic members of the LAMOX family, has been attributed either to a disordering in the oxygen sublattice or to a possible oxygen loss [28,29]. However, our thermogravimetric results show that the second hypothesis is unlikely to be at the basis of this slope change in the thermal expansion coefficient for our sample; moreover, its presence is reproduced for the two data sets (air and vacuum). Other authors [24] agree with the fact that the oxygen loss is unlikely to be at the origin of this extra volume expansion; on the contrary, they suggest a possible relation with the non-Arrhenius behaviour observed at

Table 1
Refined lattice parameters and fractional atomic coordinates (e.g. $P2_13$) for $(La_{0.95}K_{0.05})2Mo_2O_9$: neutron powder diffraction data recorded under air

|	30	400	500	600	650	700
a (Å)	7.1684(4)	7.2062(4)	7.2200(4)	7.2366(4)	7.2437(5)	7.2502(5)
La/K (4a)						
x	0.8550(5)	0.8532(5)	0.8526(6)	0.8517(6)	0.8509(6)	0.8506(6)
Mo (4a)						
x	0.1728(9)	0.1714(6)	0.1716(6)	0.1706(6)	0.1704(6)	0.1705(6)
O1 (4a)						
x	0.3146(8)	0.3136(8)	0.3144(8)	0.3142(7)	0.3142(8)	0.3139(8)
O2 (12b)						
x	0.985(1)	0.982(1)	0.982(1)	0.982(1)	0.982(1)	0.981(1)
y	0.173(2)	0.163(2)	0.159(2)	0.161(2)	0.159(3)	0.155(3)
z	0.353(1)	0.349(1)	0.344(2)	0.344(2)	0.341(2)	0.339(2)
O3 (12b)						
x	0.962(5)	0.979(5)	0.982(5)	0.984(3)	0.987(4)	0.995(4)
y	0.741(5)	0.739(4)	0.734(4)	0.737(3)	0.741(3)	0.738(3)
z	0.515(3)	0.509(3)	0.513(3)	0.507(2)	0.507(3)	0.510(3)
Rwp (%)	7.06	6.43	6.60	6.30	6.49	6.11
Rp (%)	4.99	4.61	4.61	4.55	4.54	4.46

Standard deviations given in brackets.
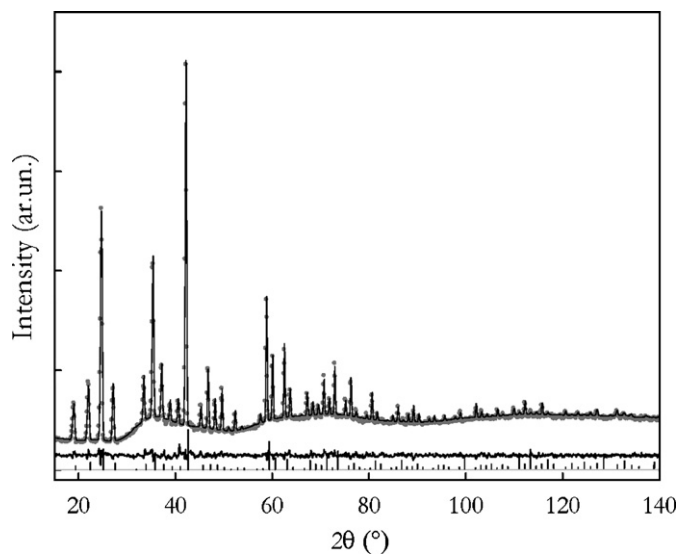
Fig. 2. Example of observed, calculated and difference profile for cubic $(La_{0.95}K_{0.05})_2Mo_2O_9$. Data acquired on D1A, ILL, under vacuum.

Fig. 4. Oxygen coordination around the cations in β-$La_2Mo_2O_9$.
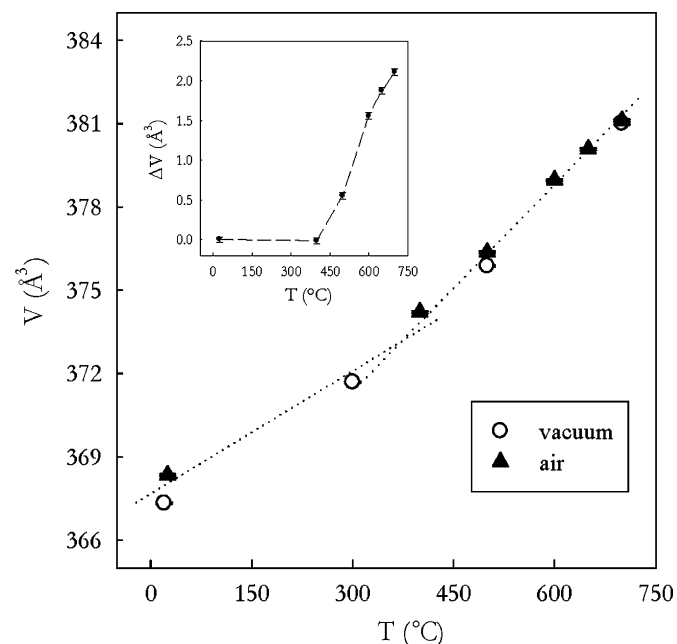

Fig. 3. Cell volume variation with temperature for cubic $(La_{0.95}K_{0.05})_2Mo_2O_{8.9}$.

high temperature for this family of ionic conductors. Thought we remark the presence of this deviation from linearity in the unit cell volume vs. temperature trend, we stress that, due to the low number of experimental data below 400 °C, its detection would probably not have been considered in the absence of the previous literature. On the other hand, as it will be discussed later, a more pronounced deviation is visible at temperature higher than 400–500 °C for other structural parameters calculated in this study.

In all the graphs presented both the data recorded in air (black triangles) and those in vacuum (empty circles) are reported for comparison. It is interesting to note that trends
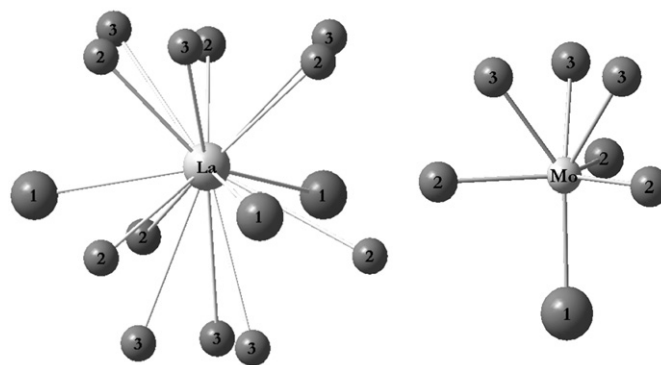
and absolute values are perfectly comparable for the two sets of data. This implies that the effect of the vacuum used during these measurements is negligible on the structural properties of these materials and supports the reliability of the results obtained in this measurement environment.

The ligand arrangement around the cations in β-$La_2Mo_2O_9$ is not straightforward to describe. In Fig. 4 the oxygen coordination around La and Mo is schematically presented. Lanthanum is surrounded by 15 oxygens (labelled as O1, O2 and O3): three O1 are placed almost in the equatorial plane; below these, three O2 (all in the same plane) can be found at a distance of about 2.7 Å and far away, at a distance of about 2.85 Å, three O3 are located. Above the equatorial plane, three O2 and three O3 ions are closer to the cation ($\sim$2.5–2.6 Å) and are at alternating positions forming something like a "circle" characterized by short O-O distances. Molybdenum is surrounded by seven oxygen ions ($\sim$1.7–1.9 Å): three O2 in the equatorial plane, one O1 placed below this plane, in an apical position, and three O3 above the equatorial plane. This representation does not take into account the thermal factors which, especially for O2 and O3, tends to be highly anisotropic; moreover, it should be remarked that O2 and O3 are partially occupied.

According to the differences in ionic radii for the two cations ($Mo^{6+} = 0.73$ Å; $La^{3+} = 1.36$ Å), the Mo polyhedron is generally smaller than the La polyhedron. This is demonstrated by the values of the average cation-oxygen distances, indicated as $\langle La–O \rangle$ and $\langle Mo–O \rangle$ respectively. The average cation-oxygen distances have been calculated taking into account the partial site occupancies of the oxygen sites, as described elsewhere [21]. The average $\langle La–O \rangle$ bond length increases linearly with temperature (Fig. 5), with a thermal expansion coefficient higher than that for the average $\langle Mo–O \rangle$ bond length over the whole temperature range considered. Again, we remark the perfectly good agreement between the two sets of data presented. Investigation of the single cation–oxygen distances reveals the following main points:

- La–O1 bond length increases linearly with temperature, as well as the average $\langle La–O2 \rangle$ and $\langle La–O3 \rangle$ distances (Fig. 6).
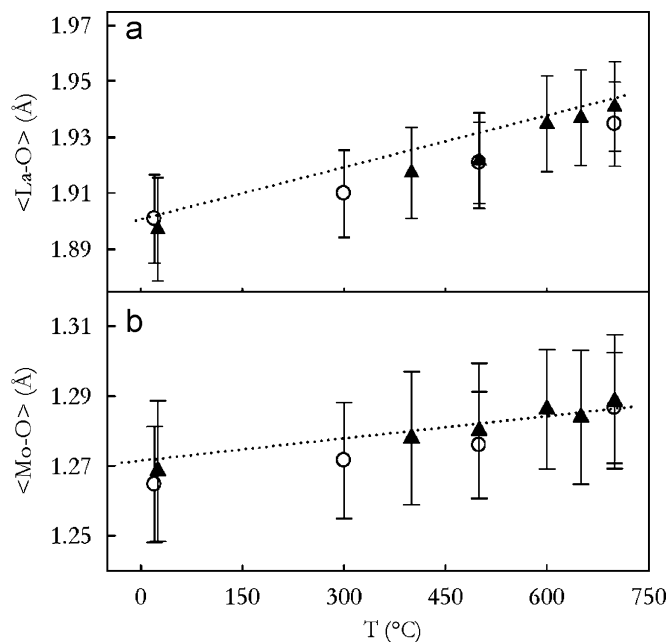
Fig. 5. Average cation–oxygen distances as a function of temperature; (a) ⟨La–O⟩ and (b) ⟨Mo–O⟩. Black symbols refer to data acquired in air, empty symbols to vacuum. Lines are guides for the eye only.
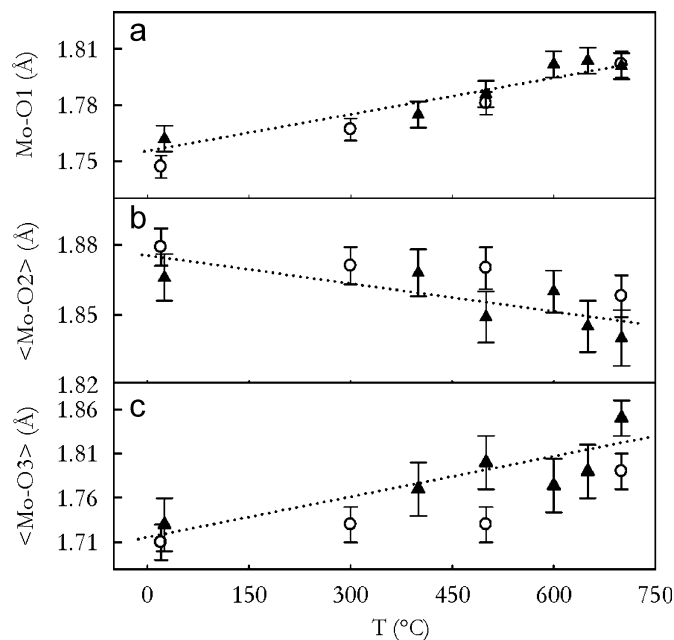

Fig. 7. Variation with temperature of the single: (a) Mo–O1 distance; (b) Mo–O2; and (c) Mo–O3 distances. Black symbols refer to data acquired in air, empty symbols to vacuum. Lines are guides for the eye only.
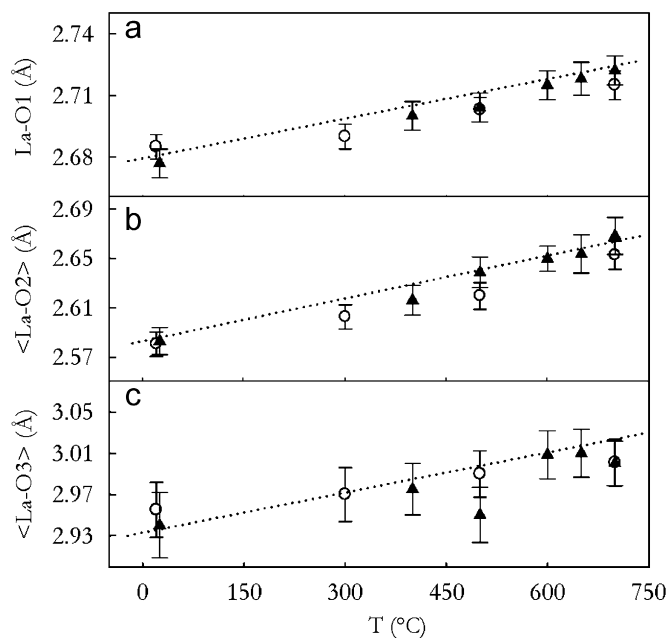

Fig. 6. Variation with temperature of: (a) single La–O1 distance; (b) average ⟨La–O2⟩ and (c) ⟨La–O3⟩ distances. Black symbols refer to data acquired in air, empty symbols to vacuum. Lines are guides for the eye only.
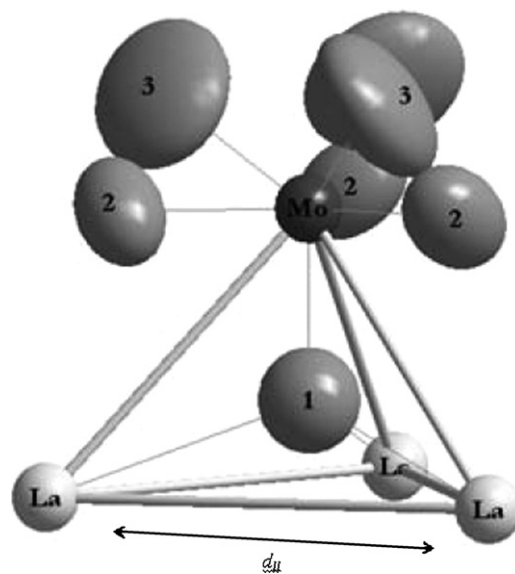

Fig. 8. Anti-tetrahedral units centred in O1, showing the disposition of the large and anisotropic thermal factors for the partial occupied oxygen sites.

- Mo–O1 and Mo–O3 bond lengths increase linearly with temperature while Mo–O2 becomes shorter as the temperature increases, varying from ~1.9 to 1.8 Å, (Fig. 7).

The shortening in Mo–O2 distances with temperature minimizes the difference between the three single Mo–O1,

Mo–O2 and Mo–O3 bond lengths, thus producing a more regular disposition of the oxygen ions around the molybdenum at high temperature.

As pointed out in the introduction, a more suitable approach to the description of the ions environment in this complex structure is based on the use of [O1LaMo] anti-tetrahedral units representing the cationic coordination around the fully occupied O1 site (Fig. 8). The advantage of this description relies on the possibility to build up a complete structural and rigid framework based only on fully occupied crystallographic sites, while the two partially

occupied oxygen sites (indicated as O2 and O3) are situated in the open channels. The opening of these channels in the high temperature range, due to the rotation and tilting of the anti-tetrahedral units, has been suggested [24] to be responsible for the extra unit cell volume expansion at high temperature. This has also been suggested to be correlated with the non-Arrhenius behaviour typical of these phases. For this reason, the tilting angle indicated as δ has been calculated, based on our experimental data, according to the following equation (as defined in Ref. [24]):

$$\tan(\delta) = \sqrt{\frac{8(d_{ll}/a)^2}{3} - 1},$$

where d_{ll} represents the distance between two adjacent La ions defining the edge of an anti-tetrahedral unit (Fig. 8) and a represents the lattice constant. The evolution with temperature of this parameter is not linear (Fig. 9). At high temperature a positive deviation from linearity, which is indeed similar to that discussed for the unit cell volume, is visible. In Table 2 the tilting angle δ, calculated on the basis of the experimental geometry of the anti-tetrahedral units obtained in this study is compared to the tilting angle δ calculated (according to Ref. [24]) by keeping the same constant geometry for the anti-tetrahedral units for the whole temperature range considered. Our results are in contrast to what was proposed by Lacorre's group [24], whose speculation is based on the assumption that the anti tetrahedral units constitute a semirigid framework in which the geometry does not change upon temperature. The data reported indicate an opposite trend for this value. Although we remark that, in order to be sure of the general validity of the experimental trend, a more

Table 2
For $(La_{0.95}K_{0.05})2Mo_2O_9$: neutron powder diffraction data recorded under air

	d_{ll}	d_{ml}	δ_{exp}	δ_{calc}
30	4.408(5)	3.633(7)	5.26	9.75
400	4.435(5)	3.672(6)	5.74	7.79
500	4.445(6)	3.679(6)	5.89	6.94
600	4.458(6)	3.699(6)	6.21	5.76
650	4.463(6)	3.709(6)	6.36	5.18
700	4.468(6)	3.713(6)	6.43	4.57

$$\tan(\delta) = \sqrt{\frac{8(d_{ll}/a)^2}{3} - 1}$$

Experimental geometry of the anti-tetrahedral units for $(La_{0.95}K_{0.05})_2$ Mo_2O_9: neutron powder diffraction data recorded under air. Experimental (this study) and calculated (according to the assumption in Ref. [24]) tilting angle δ. Standard deviations given in brackets.
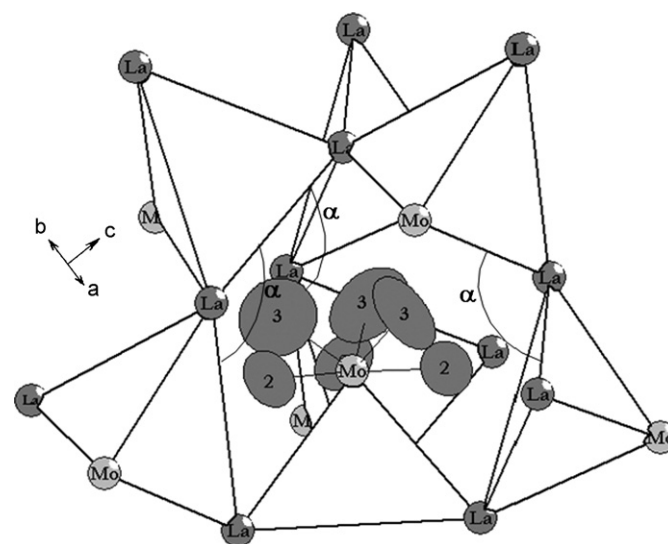

Fig. 10. Anti-tetrahedral unit centred in O1 and linked through La ions to form a cage where the partially occupied O2 and O3 ions are placed.

comprehensive study on different compositions should be performed, we stress that the fact that a first experimental set of data is in opposition with the suggestion made on the basis of molecular dynamic study is relevant.

Fig. 10 shows the disposition of the anti-tetrahedral units linked through La ions to form a cage where the partially occupied O2 and O3 ions are placed. Fig. 11 shows the evolution with temperature of the La–La–La angle indicated in Fig. 10 as α. As the temperature increases, this angle increases; this structural change is responsible for the opening of this cage with temperature. It is important to note here that the trend is similar to the one observed for the unit cell volume expansion with temperature and that a clear correlation is visible for the two parameters. It has been previously suggested [24] that any additional volume freed up by the anti-tetrahedral units rotation is likely to favour the ionic mobility or to be correlated to it. We then
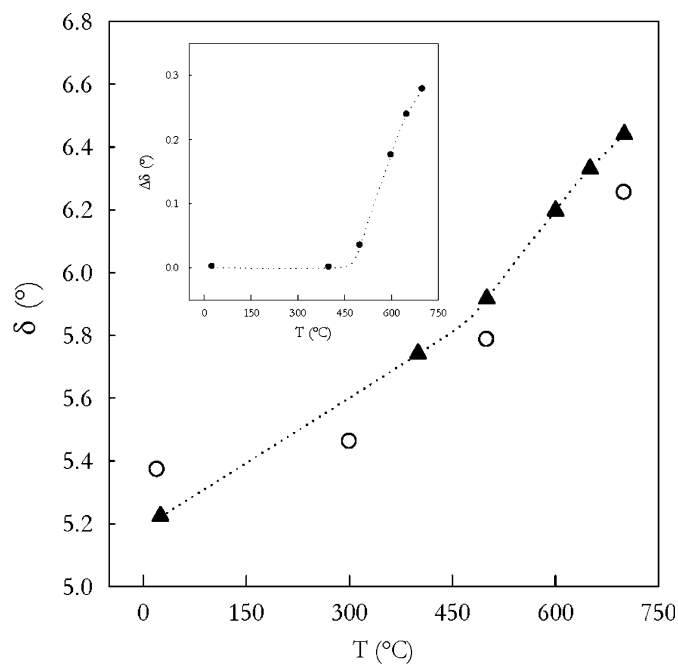

Fig. 9. Variation with temperature of the tilting angle. Black symbols refer to data acquired in air, empty symbols to vacuum.
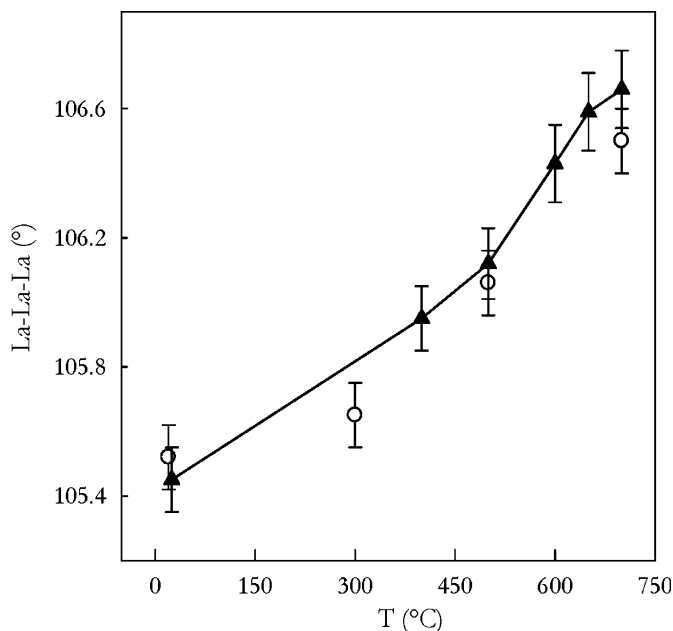
Fig. 11. Variation with temperature of the La–La–La angle responsible for the opening of the cage.
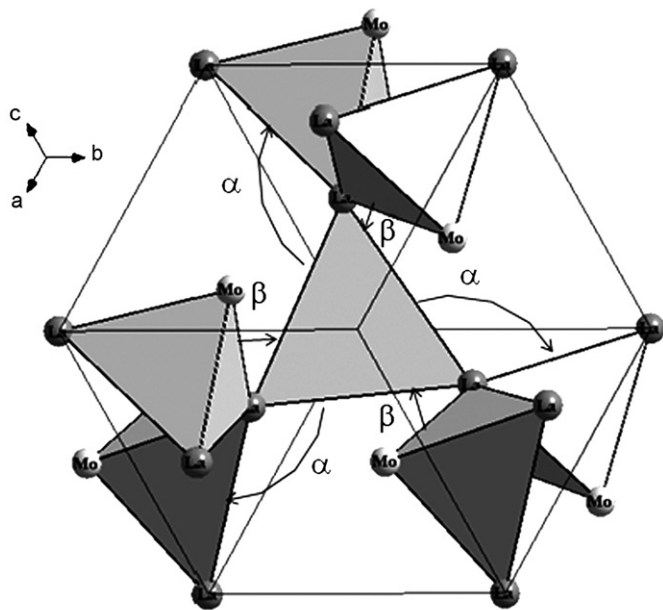

Fig. 12. Schematic representation of the cooperative motion of the anti-tetrahedral units with temperature which consists in the opening of the α angle and the reduction of β and whose result is correlated with the non linear unit cell volume expansion.

propose that the "opening" of the cage due to the anti-tetrahedral units rotation might be correlated with the high temperature non-Arrhenius behaviour typical of these phases. Moreover, the opening of this cage might be responsible for the extra unit cell volume expansion observed experimentally. Fig. 12 is a schematic representation of the cooperative motion of the anti-tetrahedral units with temperature which consists in the opening of the La–La–La angle (α) and the reduction of the La–La–Mo

angle (β) and whose result is correlated with the non linear unit cell volume expansion.

4. Conclusions

This study presents a detailed structural analysis of a cubic $La_2Mo_2O_9$ sample. The evolution with temperature of selected structural parameters suggests a correlation with the experimentally observed decrease of the activation energy for oxygen migration at high temperature.

The main results of this study can be summarised as follows:

- The effect of vacuum on the structural properties of K-doped cubic $La_2Mo_2O_9$ is negligible. The perfect agreement between data acquired in air and under vacuum ensures the structural stability of the sample at low oxygen partial pressure.
- The unit cell volume of cubic K-doped $La_2Mo_2O_9$ increases as the temperature increases, with a relevant deviation from the linear trend for temperatures higher than approximately 400 °C.
- The average $\langle La–O \rangle$, which according to the differences in ionic radii is larger than $\langle Mo–O \rangle$, increases linearly with temperature; this behaviour is the result of a regular expansion of both the single La–O1 distance and the average $\langle La–O2 \rangle$ and $\langle La–O3 \rangle$ bond lengths.
- The average $\langle Mo–O \rangle$ increases with temperature as a result of a regular expansion of the Mo–O1 and Mo–O3 bond length and a compression of the Mo–O2 distance. The shortening in Mo–O2 distances with temperature minimizes the difference between the three single Mo–O1, Mo–O2 and Mo–O3 bond lengths, thus producing a more regular disposition of the oxygen ions around the molybdenum at high temperature.
- The evolution with temperature of relevant tilting angles between anti-tetrahedral units corresponds to the opening with temperature of the cage where O2 and O3 ions, supposed mobile species in this structure, are located. This can be correlated to the extra unit cell volume expansion and to the appearance of the non-Arrhenius regime at high temperature.

The structural stability of the system, ensured by the absence of relevant modifications at the low oxygen partial pressure applied during these measurements, represents a valuable information in view of possible applications of this material in solid state devices. Of course, more important for the actual application of Lamox-based materials as electrolyte in solid oxide fuel cell is their stability against reduction at low oxygen partial pressure, with the presence of an ionic domain as large as possible at the foreseen operating temperature. However, information on the transport properties needs to be coupled with a known structural stability, especially because these are important supporting information for the comprehension of the properties of this material. The set of results

presented, although probably not definitive on the interpretation of the complicated relationships between structural features and transport properties of this fascinating oxide, represents an interesting starting point for further structural tests.

Appendix A. Supplementary information

Supplementary data associated with this article can be found in the online version at doi:10.1016/j.jssc.2008.01.001.

References

[1] P. Lacorre, F. Goutenoire, O. Bohnke, R. Retoux, Y. Laligant, Nature 404 (2000) 856.
[2] P. Lacorre, Solid State Sci. 2 (2000) 755.
[3] X.P. Wang, Q.F. Fang, Z.S. Li, G.G. Zhang, Z.G. Yi, Appl. Phys. Lett. 81 (2002) 3434.
[4] Z.S. Khadasheva, N.U. Venskovskii, M.G. Safronenko, A.V. Mosunov, E.D. Politova, S.Y. Stefanovich, Inorg. Mater. 38 (2002) 1168.
[5] J.A. Collado, M.A.G. Aranda, A. Cabeza, P. Olivera-Pastor, S. Bruque, J. Solid State Chem. 167 (2002) 80.
[6] S. Georges, F. Goutenoire, Y. Laligant, P. Lacorre, J. Mater. Chem. 13 (2003) 2317.
[7] D. Marrero-Lopez, J. Canales-Vazquez, J.C. Ruiz-Morales, J.T.S. Irvine, R. Nunez, Electrochim. Acta 50 (2005) 4385.
[8] R. Subasri, D. Matusch, H. Nafe, F. Aldinger, J. Eur. Ceram. Soc. 24 (2004) 129.
[9] C. Tealdi, G. Chiodelli, L. Malavasi, G. Flor, J. Mater. Chem. 14 (2004) 3553.
[10] F. Goutenoire, O. Isnard, P. Lacorre, Chem. Mater. 12 (2000) 2575.
[11] S. Georges, F. Goutenoire, F. Altorfer, D. Sheptyakov, F. Fauth, E. Suard, P. Lacorre, Solid State Ionics 161 (2003) 231.
[12] I.R. Evans, J.A.K. Howard, J.S.O. Evans, Chem. Mater. 17 (2005) 4074.
[13] L. Malavasi, H.J. Kim, S.J.L. Billinge, T. Proffen, C. Tealdi, G. Flor, J. Am. Chem. Soc. 129 (2007) 6903.
[14] X.P. Wang, Q.F. Fang, Phys. Rev. B65 (2002) 064304.
[15] Z.G. Yi, Q.F. Fang, X.P. Wang, G.G. Zhang, Solid State Ionics 160 (2003) 117.
[16] Q.F. Fang, X.P. Wang, G.G. Zhang, Z.G. Yi, J. Alloys Compds. 355 (2003) 177.
[17] X.P. Wang, Z.J. Cheng, Q.F. Fang, Solid State Ionics 176 (2005) 761.
[18] F. Goutenoire, O. Isnard, E. Suard, O. Bohnke, Y. Laligant, R. Retoux, P. Lacorre, J. Mater. Chem. 11 (2001) 119.
[19] S. Georges, S.J. Skinner, P. Lacorre, M.C. Steil, Dalton Trans. 19 (2004) 3101.
[20] C.J. Hou, Y.D. Li, P.J. Wang, C.S. Liu, X.P. Wang, Q.F. Fang, D.Y. Sun, Phys. Rev. B76 (2007) 014104.
[21] G. Corbel, Y. Laligant, F. Goutenoire, E. Suard, P. Lacorre, Chem. Mater. 17 (2005) 4678.
[22] M. O'keeffe, B.G. Hyde, Struct. Bonding 61 (1985) 77.
[23] S. Georges, F. Goutenoire, O. Bohnke, M.C. Steil, S.J. Skinner, H.D. Wiemhofer, P. Lacorre, J. New Mater. Electrochem. Systems 7 (2004) 51.
[24] P. Lacorre, A. Selmi, G. Corbel, B. Foulard, Inorg. Chem. 45 (2006) 627.
[25] S. Georges, O. Bohnké, F. Goutenoire, Y. Laligant, J. Fouletier, P. Lacorre, Solid State Ionics 177 (2006) 1715.
[26] H.M. Rietveld, Acta Cryst. 22 (1967) 151.
[27] H.M. Rietveld, J. Appl. Cryst. 2 (1969) 65.
[28] I.P. Marozau, A.L. Shaula, V.V. Kharton, N.P. Vyshatko, A.P. Viskup, J.R. Frade, F.M.B. Marques, Mater. Res. Bull. 40 (2005) 361.
[29] I.P. Marozau, D. Marrero-Lopez, A.L. Shaula, V.V. Kharton, E.V. Tsipis, J.R. Frade, Electrochim. Acta 49 (2004) 3517.
[30] J. Rodriguez-Carvajal, Physica B 192 (1993) 55.